Quantum Hall effect in monolayer-bilayer graphene planar junctions

Jifa Tian,[1,2,*] Yongjin Jiang,[1,3] Isaac Childres,[1,2] Helin Cao,[1,2] Jiangping Hu,[1] and Yong P. Chen[1,2,4,†]

[1]*Department of Physics, Purdue University, West Lafayette, Indiana 47907, USA*

[2]*Birck Nanotechnology Center, Purdue University, West Lafayette, Indiana 47907, USA*

[3]*Center for Statistical and Theoretical Condensed Matter Physics, and Department of Physics, Zhejiang Normal University, Jinhua 321004, People's Republic of China*

[4]*School of Electrical and Computer Engineering, Purdue University, West Lafayette, Indiana 47907, USA*

(Received 25 March 2013; revised manuscript received 13 August 2013; published 6 September 2013)

The Hall resistance of a homogeneous electron system is well known to be antisymmetric with respect to the magnetic field and the sign of charge carriers. We have observed that such symmetries no longer hold in planar hybrid structures consisting of partly single layer graphene (SLG) and partly bilayer graphene (BLG) in the quantum Hall (QH) regime. In particular, the Hall resistance across the SLG and BLG interface is observed to exhibit quantized plateaus that switch between those characteristic of SLG QH states and BLG QH states when either the sign of the charge carriers (controlled by a back gate) or the direction of the magnetic field is reversed. Simultaneously reversing both the carrier type and the magnetic field gives rise to the same quantized Hall resistances. The observed SLG-BLG interface QH states, with characteristic asymmetries with respect to the signs of carriers and magnetic field, are determined only by the chirality of the QH edge states and can be explained by a Landauer-Büttiker analysis applied to such graphene hybrid structures involving two regions of different Landau level structures.

DOI: 10.1103/PhysRevB.88.125410 PACS number(s): 73.43.Fj, 71.70.Di, 73.22.Pr, 73.23.−b

The success of isolating single layer carbon lattices (graphene) has opened an exciting research field for both fundamental physics and potential nanoelectronic devices applications.[1–5] Graphene exhibits an unusual band structure showing a linear relationship between the energy and the momentum near the Dirac point and allowing electric field tuning of both the type and the density of charge carriers, which are massless Dirac fermions capable of reaching impressively high mobilities.[1,6–9] Previous studies have demonstrated that single layer graphene (SLG) shows a half-integer quantum Hall effect (QHE), where the Hall resistance is quantized at values of $R_{xy} = h/\nu_1 e^2$ around filling factors $\nu_1 = \pm 4(N + 1/2)$.[2,3] Here, N is an integer, e is the electron charge, h is Planck's constant, and the factor 4 is due to spin and valley degeneracy. Bilayer graphene (BLG), composed of two graphene monolayers weakly coupled by interlayer hopping, is also interesting and has been shown to have additional unique physical properties.[10–12] Charge carriers in BLG (assuming normal AB stacking) are massive chiral fermions with Berry's phase 2π.[10] BLG is observed to display integer QHE of quantized Hall plateaus $R_{xy} = h/\nu_2 e^2$ around filling factors $\nu_2 = \pm 4N$.

It is well known that the Hall resistance (R_{xy}) of a homogenous electron system is antisymmetric with respect to carrier density (n, where positive n refers to holes and negative n refers to electrons) and magnetic field (B); i.e., $R_{xy}(-n/B) = -R_{xy}(n/B)$. Such electron-hole ($e$-$h$) and B symmetries in the Hall transport are also obeyed in QHE observed in two-dimensional electron systems (2DES) in general,[13] including the QHE for both SLG and BLG.[2,3,10] We will show in this paper that such a familiar symmetry is violated in a remarkable way in a SLG-BLG hybrid planar structure (even when the carrier density n may be uniform).

A SLG-BLG hybrid planar structure consists of partly SLG and partly BLG. As the SLG and BLG parts possess qualitatively different electronic band structures, such a planar heterostructure between two segments with different Landau level (LL) sequences (and different Berry's phases for charge carriers[5]) is fundamentally interesting, with no analog in conventional 2DES, and may result in novel physics and transport properties. While the QHE of either SLG or BLG has been extensively studied, hybrid SLG-BLG structures[14–18] have received relatively little attention. A recent theoretical article predicted rich structures in the interface LL in a SLG-BLG junction, but its transport properties have not been studied.[15] Experimentally, Puls *et al.* studied the quantum oscillations and observed various anomalous features in two-terminal magnetoresistance parallel to the interface of hybrid SLG-BLG structures.[14] Unusual features in the two-terminal magnetoconductance[17] and a longitudinal resistance (R_{xx}) asymmetric in the signs of carriers and magnetic field have been observed across SLG-BLG interfaces.[18] To our knowledge, however, there is no experimental work reported on the interface QHE (especially the Hall resistance) in a SLG-BLG hybrid structure. Here, we report on a systematic study of quantum Hall (QH) transport in such junctions and the observation of interface QH states, where none of the usual e-h and B symmetries are obeyed. The interface QH plateaus are found to switch between SLG-like and BLG-like values when either n or B is reversed. We also present a theoretical model using a Landauer-Büttiker analysis to explain the main observations.

Our hybrid structures, consisting of partial SLG and BLG, are mechanically exfoliated from highly ordered pyrolytic graphite (grade ZYA, Momentive Performance Materials), transferred onto a wafer with 280-nm thermal oxide (SiO_2) on top of a p^{++} Si substrate,[19] and selected by the optical contrast[20] and Raman spectra[21] of SLG and BLG flakes. A typical optical image of a hybrid SLG-BLG structure is shown in Fig. 1(a). Some representative Raman spectra of the SLG and BLG parts are shown in Fig. 1(b). We use a standard e-beam lithography process[19] to fabricate devices with various

 ©2013 American Physical Society

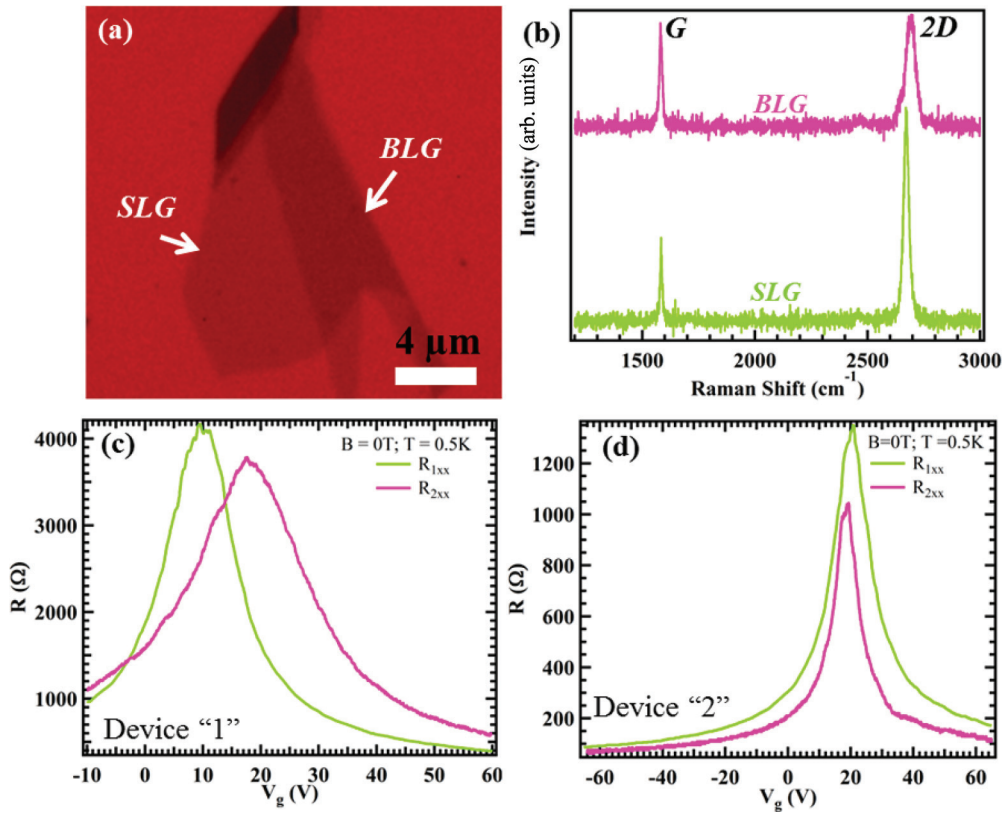

FIG. 1. (Color online) (a) Optical image of a SLG and BLG hybrid structure (exfoliated from graphite). (b) Representative Raman spectra of the SLG and BLG parts in device 1. The wavelength of the Raman excitation laser is 532 nm. The power of the laser is ∼200 μW incident on the sample. The field effect curves (R vs V_g) are measured from the SLG (R_{1xx}) and BLG (R_{2xx}) parts for (c) device 1 and (d) device 2.

geometries. Two devices [numbered 1 and 2 and shown in Figs. 2(a) and 3(a)], will be presented in this article. The measurements are performed in a helium-3 system with B up to ± 18 T. At $B = 0$ T and $T = 0.5$ K, we performed field effect measurements (four-terminal resistance R vs back gate voltage V_g) on both the SLG and the BLG parts in devices 1 and 2. The corresponding results are shown in Figs. 1(c) and 1(d), respectively. In device 1, the charge neutrality points (CNPs) are $V_{1\mathrm{CNP}} \approx 10$ V and $V_{2\mathrm{CNP}} \approx 17$ V for the SLG and BLG parts, respectively. For device 2, the measured V_{CNP} of both the SLG and the BLG parts are ∼20 V. There can be slight hysteresis and variations (∼2 V) in V_{CNP} in our devices for different gate sweeps and measurements.

Figures 2(a) and 2(b) shows the optical image and corresponding schematic three-dimensional (3D) structure of device 1, where SLG and BLG are connected in series between the drain (D) and the source (S) electrodes. In this device, the Hall and longitudinal resistances of the SLG part (R_{1xy} and R_{1xx}), BLG part (R_{2xy} and R_{2xx}), and SLG-BLG interface (R_{12xy} and R_{12xx}) can all be measured simultaneously. The measured low field magnetoresistance and Hall resistances of both SLG and BLG parts are also used to extract their carrier densities and Hall mobilities. At $V_g = 0$ V, the carrier (hole) density of the SLG part (p_{SLG}) is $\sim 9 \times 10^{11}$ cm^{-2}, and the Hall mobility (μ_{SLG}) is ∼3100 cm^2/Vs. The carrier density of the BLG part (p_{BLG}) is $\sim 1.8 \times 10^{12}$ cm^{-2}, and the mobility (μ_{BLG}) is ∼1800 cm^2/Vs. Figure 2(c) shows the Hall resistances (R_{1xy}, R_{2xy}, and R_{12xy}) and longitudinal resistances (R_{1xx}, R_{2xx}, and R_{12xx}) as functions of back gate voltages (V_g) at $B = +15$ T. The corresponding edge state chiralities,[13] either clockwise (CW) or anticlockwise (ACW), are labeled near representative QH plateaus. In the SLG part, we observe a series of well-developed QH plateaus in R_{1xy} at $\pm h/2e^2$, $\pm h/6e^2$, and $\pm h/10e^2$, where the corresponding R_{1xx} are vanishing. We also observe QH states from the BLG part with R_{2xy} quantized at $\pm h/4e^2$, $h/8e^2$, and $h/12e^2$. These results indicate that the characteristic QHEs observed in SLG or BLG are still preserved in the SLG and BLG parts of the graphene hybrid structures and obey e-h symmetry. Interestingly, the Hall resistance R_{12xy} of the SLG-BLG interface also shows quantized plateaus. In particular, when the charge carriers are holes ($V_g < \sim 10$ V), R_{12xy} is observed to closely resembles BLG R_{2xy} and displays a well-developed plateau at $h/4e^2$, as well as other developing plateaus near $h/8e^2$ and $h/12e^2$, all corresponding to the values of BLG QH states. However, when the carriers are changed to electrons for $V_g > \sim 20$ V, R_{12xy} shows a developing plateau close to $-h/2e^2$, a value corresponding to a SLG QH state. Alternatively, we can measure the QHE by tuning B at a fixed V_g. Figure 2(d) shows the results of such measurements at $V_g = 0$ V (where the carriers are holes in both parts). The Hall resistance R_{1xy} (R_{2xy}) of the SLG (BLG) part exhibits characteristic SLG (BLG) QH states near ± 15 T with well-defined plateaus at $\pm h/2e^2$ ($\pm h/4e^2$) accompanied by vanishing R_{1xx} (R_{2xx}), showing that the QHEs measured in the SLG and BLG parts are individually symmetric with B. The interface R_{12xy} also shows well-defined

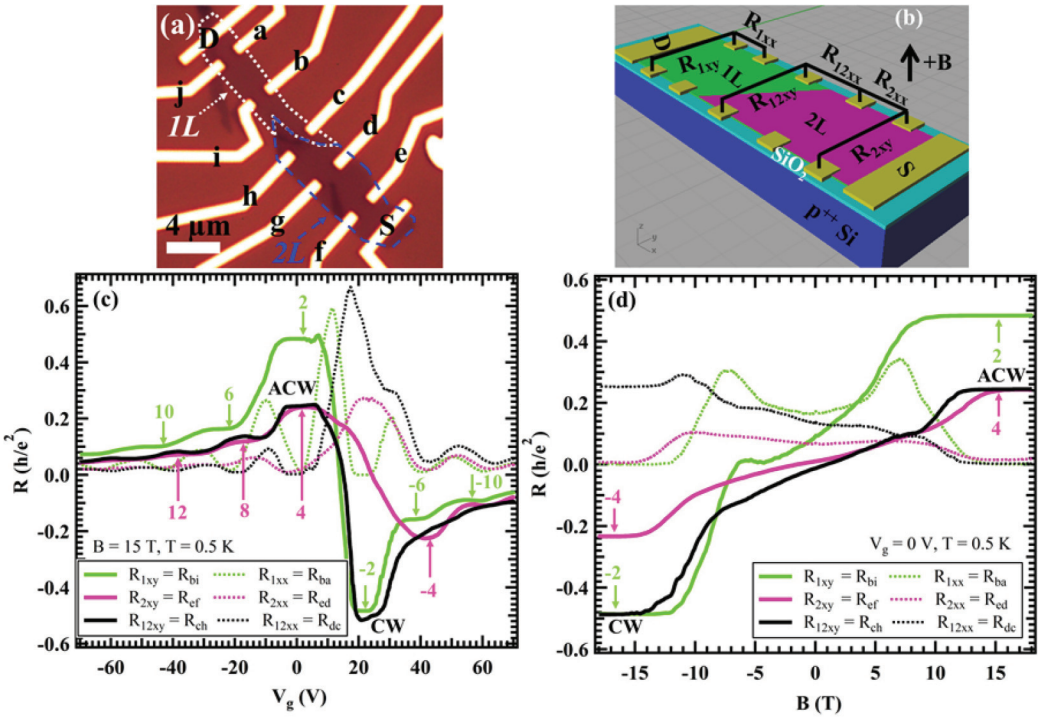

FIG. 2. (Color online) (a) Optical image of device 1. The contours for the regions corresponding to SLG and BLG are highlighted by white dotted and blue dashed lines, respectively. The widths of all electrodes are 1 μm. (b) Schematic 3D structure of the device, indicating electrical connections for various resistance measurements. The positive B direction (black arrow) points upward. (c) Hall resistances (R_{1xy}, R_{2xy}, and R_{12xy}) and longitudinal resistances (R_{1xx}, R_{2xx}, and R_{12xx}), as functions of V_g at $B = +15$ T and $T = 0.5$ K. (d) R_{1xy}, R_{2xy}, and R_{12xy}, as well as R_{1xx}, R_{2xx}, and R_{12xx}, as functions of the B at 0.5 K and $V_g = 0$ V. In (c) and (d), QH plateaus associated with SLG or BLG QH states are labeled by arrows, and their quantum numbers (m, related to the plateau values $R_{xy} = h/(me^2)$) are green or purple, respectively. The edge state chirality, CW or ACW, has been labeled near the representative QH plateaus observed in R_{12xy} in both (c) and (d).

quantized Hall plateaus; however, they are asymmetric upon the reversal of the B. Near $+15$ T, R_{12xy} shows a quantized plateau at $h/4e^2$ corresponding to a BLG QHE, accompanied by a vanishing R_{12xx}. However, near -15 T, R_{12xy} is quantized at $-h/2e^2$ (the value for a SLG QHE) with accompanying R_{12xx} now displaying a resistance plateau (at $h/4e^2$) rather than vanishing. The observation [Figs. 2(c) and 2(d)] that the quantized R_{12xy} switch between SLG-like and BLG-like values when either the carrier type or the B field is reversed implies that simultaneous reversing both the carrier type and the B field would give rise to the same quantized R_{12xy} [e.g., the SLG-like QH plateau of $-h/2e^2$ seen for both electrons, $+15$ T in Fig. 2(c), and holes, -15 T in Fig. 2(d)]. Our results also suggest that the interface QH states and their quantized Hall plateau values are determined by the chirality of edge state currents [e.g., in Figs. 2(c) and 2(d), the BLG-like QH plateaus are observed with ACW edge state chirality, whereas the SLG-like QH plateau ($-h/2e^2$) is observed with CW edge state chirality].

Qualitatively similar results are observed in device 2 [Figs. 3(a) and 3(b)]. Here, the D electrode connects to both the SLG and the BLG parts and the S electrode is touching the SLG only. We mainly focus on the Hall resistance R_{12xy} crossing the interface (measured between electrodes c and b). The measured $V_{\rm CNP}$ of both the SLG and the BLG parts is $\sim$20 V. Due to its structure and electrode configuration, device 2 does not allow measurement of individual Hall effects from its SLG and BLG parts. We can extract an effective density for holes of $\sim 1.8 \times 10^{12}$ cm^{-2} from low-B R_{12xy} and a mobility (μ, using R_{xx} measured between a and b in the SLG part) to be $\sim$7200 cm^2/Vs at $V_g = 0$. In Fig. 3(c), we again see that R_{12xy} (as a function of V_g at $B = \pm 18$ T) shows quantized plateaus that switch between SLG-like and BLG-like QH plateau values when reversing the sign of carriers. For example, when $B = -18$ T, R_{12xy} exhibits plateaus at $-h/10e^2$, $-h/6e^2$, and $-h/2e^2$ (values of SLG QH states) for $V_g < V_{\rm CNP}$ (holes) but exhibits plateaus at $+h/4e^2$ and $+h/8e^2$ (values of BLG QH states) for $V_g > V_{\rm CNP}$ (electrons). By reversing the B field (thus changing the chirality of the edge state currents), the relatively well-developed quantized Hall plateaus of R_{12xy} now switch from BLG-like QH plateaus ($+h/12e^2$, $+h/8e^2$, and $+h/4e^2$) to SLG-like QH plateaus ($-h/2e^2$ and $-h/6e^2$) as carriers switch from holes to electrons. It is also notable that the values of the relatively well-developed SLG-like QH plateaus in R_{12xy} tend to be negative (CW edge state chirality), whereas those corresponding to BLG-like QH states tend to be positive (ACW edge state chirality). This is again confirmed by the B-dependent R_{12xy} shown in Fig. 3(d). In particular, we observe the SLG-like plateau developing at $-h/2e^2$ for holes ($V_g = 0$ V $< V_{\rm CNP}$) near $B = -18$ T and well developed for electrons ($V_g = 30$ V $> V_{\rm CNP}$) near $B = +18$ T (both CW edge state chirality) and the BLG-like plateau developing at $+h/4e^2$ for holes ($V_g = 0$ V) near $B = +18$ T and well developed for electrons ($V_g = 30$ V) near $B = -18$ T (both ACW edge state

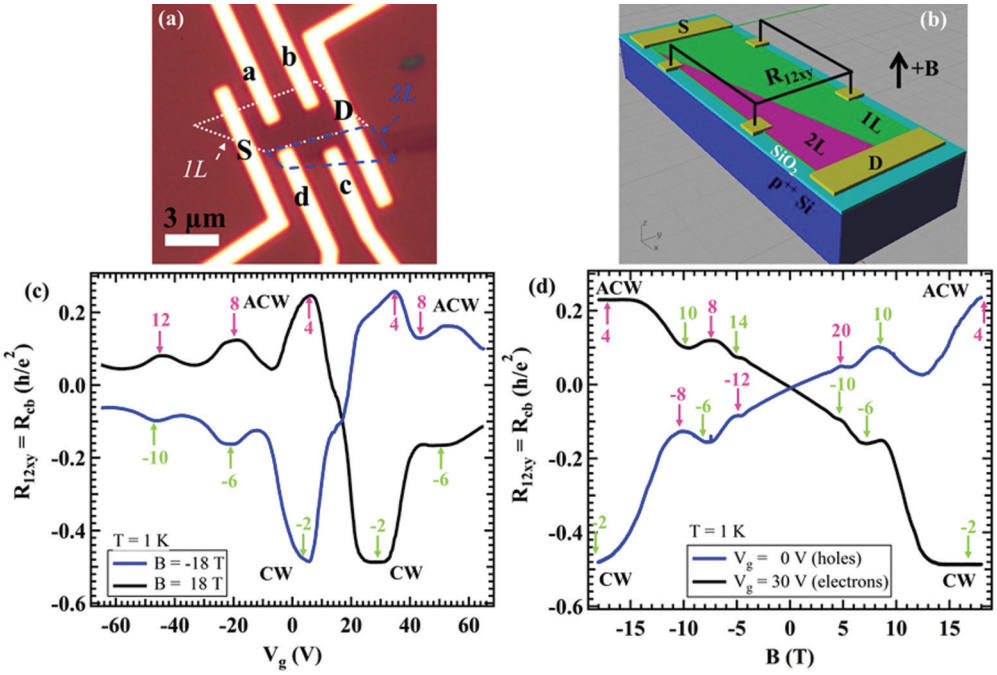

FIG. 3. (Color online) (a) Optical image of device 2. The widths of all electrodes are 1 μm. (b) Schematic 3D structure of the device with the corresponding electrical connections. (c) R_{12xy} (between electrodes c and b) as a function of V_g at $B = -18$ T and $B = +18$ T (blue and black curves, respectively). (d) R_{12xy} as a function of the B at $V_g = 0$ and 30 V (blue and black curve, respectively). In (c) and (d), QH plateaus corresponding to values associated with SLG or BLG QH states are labeled by arrows, and their quantum numbers are green or purple, respectively.

chirality). In Fig. 3(d), at lower B, R_{12xy} can show developing plateaus of both SLG-like and BLG-like values (as labeled in the figure) even with the same carrier type and B direction (e.g., for $V_g = 30$ V, electrons, and $B < 0$, we see plateaus around $h/10e^2$ and $h/14e^2$, corresponding to SLG-like QH plateau values, in addition to BLG-like $h/4e^2$ and $h/8e^2$). Such a "mixed" appearance is not fully understood, and possible reasons are discussed later.

The main features of the observed SLG-BLG interface QHE can be understood using a Landauer-Büttiker[22,23] analysis of the chiral edge states. We first consider a generic hybrid structure, consisting of two regions at different QH states [Figs. 4(a) and 4(b)]. A similar model has been analyzed for a four-terminal SLG p-n junction in Ref. 24. Figures 4(a) and 4(b) shows measurement schematics with CW and ACW edge currents, respectively. Here, we assume that the two regions are in a QH state with the number of edge states m_1 and m_2 (both regions having quantized Hall resistances $R_{SD,ae} = (V_a - V_e)/I_{SD} = h/m_1e^2$ and $R_{SD,cb} = h/m_2e^2$, with $m < 0$ for CW edge state chirality and $m > 0$ for ACW chirality). The S-D current I_{SD} is

$$I_{SD} = \frac{e^2}{h}(V_S - V_D)\cdot \min(|m_1|,|m_2|) = \frac{e^2}{h}(V_S - V_D)\cdot |m_1| \tag{1}$$

[we here assume $m_1 \cdot m_2 > 0$ and $|m_2| > |m_1|$, corresponding to the most typical situation in our SLG-BLG hybrid structures, see also Fig. 4(c)].[25] The only difference between Figs. 4(a) and 4(b) is the edge state chirality, determined by the sign of charge carriers and direction of the B field (reversing either of them reverses the chirality, while reversing both leads to the same chirality). In this case, either electrons under $+B$ or holes under $-B$ give CW edge currents, whereas electrons under $-B$ or holes under $+B$ give ACW edge currents (the QH edge state chirality is opposite to the chirality of the cyclotron orbits[22,23]). Using a Landauer-Büttiker analysis, one can calculate[24] the longitudinal resistance for the interface to be

$$R_{SD,ca} = \frac{V_c - V_a}{I_{SD}} = \begin{cases} (1/m_2 - 1/m_1)h/e^2, \text{ CW} \\ 0, \text{ ACW} \end{cases} \tag{2a}$$

$$R_{SD,be} = \frac{V_b - V_e}{I_{SD}} = \begin{cases} 0, \text{ CW} \\ (1/m_1 - 1/m_2)h/e^2, \text{ ACW} \end{cases} \tag{2b}$$

However, the interface Hall resistances are

$$R_{SD,ab} = \frac{V_a - V_b}{I_{SD}} = h/(\max(m_1,m_2)e^2) = \begin{cases} h/m_1e^2 = -h/|m_1|e^2, \text{ CW} \\ h/m_2e^2 = h/|m_2|e^2, \text{ ACW} \end{cases} \tag{3a}$$

$$R_{SD,ce} = \frac{V_c - V_e}{I_{SD}} = h/(\min(m_1,m_2)e^2) = \begin{cases} h/m_2e^2 = -h/|m_2|e^2, \text{ CW} \\ h/m_1e^2 = h/|m_1|e^2, \text{ ACW} \end{cases} \tag{3b}$$

Equations (2b) and (3b) can also be obtained from Eqs. (2a) and (3a) by reflecting the device with respect to the S-D axis.[25] In addition, the interface Hall resistance R_{12xy} can be obtained from interface longitudinal resistance [Eq. (2)] as $R_{12xx} + R_{xy}$(SLG/BLG) (e.g., $R_{SD,ab} = R_{SD,ac} + R_{SD,cb}$).

Now we apply these analyses to the SLG-BLG hybrid structure, with the SLG and BLG parts corresponding to

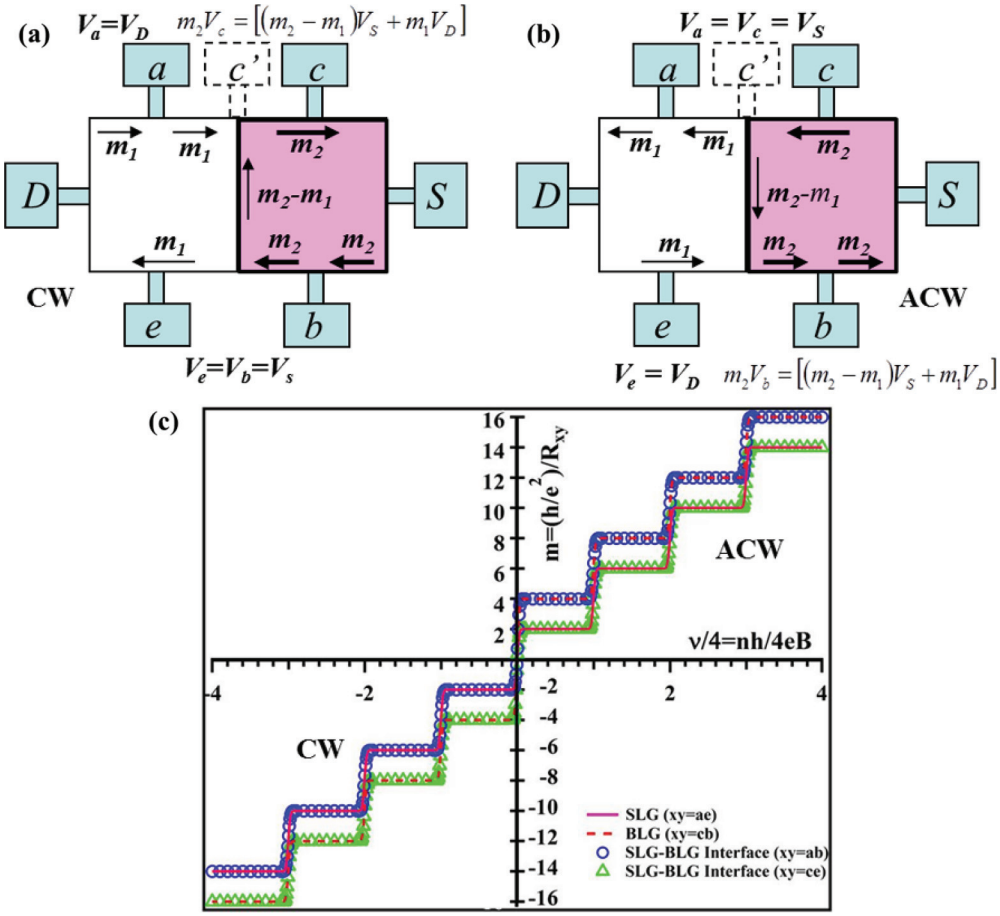

FIG. 4. (Color online) Schematic of the edge state currents with (a) CW and (b) ACW circulation in both region 1 (white) and region 2 (purple). (c) Schematic illustration of the QHE in SLG, BLG, and the SLG-BLG interface. The QHE R_{xy} of either SLG (solid line) or BLG (dashed line) is related to the corresponding number (m) of edge states in SLG or BLG by $m=(h/e^2)/R_{xy}$, where h/e^2 the resistance quantum. The calculated interface QHE R_{xy} takes the SLG or BLG values depending on the pair of electrodes used and the edge state chirality. While it is well known that $1/R_{xy}$ shows a jump of $4e^2/h$ for SLG and $8e^2/h$ for BLG at $\nu=0$ (within a single-particle physics picture), the jump for the SLG-BLG interface is $6e^2/h$.

regions 1 and 2, respectively. The configuration of device 1 (Fig. 2) is the same as that shown in [Figs. 4(a) and 4(b)]. Equation (2a) agrees well with the observed interface $R_{12xx}=h/4e^2$ at $B=-15$ T (where $m_2=-4$ and $m_1=-2$ with CW circulation), as well as $R_{12xx}=0$ at $B=+15$ T (where $m_2=4$ and $m_1=2$ with ACW circulation) in Fig. 2(d). Equations (3a) and (3b) for a SLG-BLG hybrid structure can be summarized in Fig. 4(c), showing the schematic illustration of the QHE in SLG, BLG, and the SLG-BLG interface (assuming a SLG-BLG hybrid structure with uniform n or ν). It can be seen that $|m_2|$ is always larger than $|m_1|$ at the same filling factor. It also clearly shows that the edge chirality induced switching between SLG-like and BLG-like QH plateau values in the interface quantized Hall resistances. For $R_{SD,ab}$ (corresponding to experimentally measured R_{ch} in device 1), the CW edge chirality gives rise to SLG-like QH plateaus, whereas ACW chirality gives rise to BLG-like QH plateaus. All these are again in agreement with the experimental observations [Figs. 2(c) and 2(d)].[26] For example, Fig. 2(d) shows $R_{12xy}=h/4e^2$ at $B=+15$ T (where $m_1=2$ and $m_2=4$ with ACW circulation) and $R_{12xy}=-h/2e^2$ at $B=-15$ T (where $m_1=-2$, $m_2=-4$ with CW circulation), as predicted by Eq. (3) and Fig. 4(c). In addition, the observed interface QHE could depend on the electrode pair used in the measurements. Instead of using electrodes a and b as the Hall electrodes, the measured quantized Hall resistance between electrodes c and e will show reversed switching behavior [Fig. 4(c)].

Our analysis can also be extended to device 2. From Figs. 4(a) and 4(b), we can get the geometry for device 2 by moving probe c leftward (probe c') to cover the interface (i.e., touching both SLG and BLG parts, as in device 2). The voltage V_c measured by probe c is unchanged by this movement. The configuration of device 2 (electrodes S, D, c, and b in Fig. 3(a), measuring R_{12xy}) can be realized by electrodes e, c', S, and D in Figs. 4(a) and 4(b). Using the Onsager relation that holds for four-terminal measurements in the linear response regime:

$$R_{SD,ec'}(\mathrm{CW/ACW}) = R_{ec',SD}(\mathrm{ACW/CW}) = R_{12xy}(\mathrm{ACW/CW}) \quad (4)$$

From the Hall resistance, $R_{SD,ec'} = \frac{V_e - V_{c'}}{I_{SD}} = -R_{SD,ce}$ [Eq. (3b)], we can get

$$R_{12xy}(\mathrm{ACW}) = -R_{SD,ce}(\mathrm{CW}) = \frac{h}{|m_2|e^2}$$
$$R_{12xy}(\mathrm{CW}) = -R_{SD,ce}(\mathrm{ACW}) = -\frac{h}{|m_1|e^2} \quad (5)$$

These results are consistent with the better-developed interface QH plateau resistances R_{12xy} of device 2 [Figs. 3(c) and 3(d)].

The theoretical plot in Fig. 4(c) is drawn assuming the SLG and BLG parts have the same and uniform Landau filling factor (ν). However, in real samples, spatially nonuniform doping, charge transfer, or both between the SLG and the BLG parts may result in spatially nonuniform charge carrier densities and thus different or nonuniform ν in SLG and BLG regions. Nonetheless, similar model and calculations as presented above can apply whenever the SLG and the BLG QHE plateaus overlap (which is the case for the well-developed interface QHE states observed in device 1). However, if the QH states in the two regions do not appear simultaneously, then the interface QH states will not be well developed. In addition, complicated edge state configurations at the interface have been predicted, arising from the interface LL structures (which could depend sensitively on interface orientation and disorder).[15] These factors may result in less well-developed interface QH states and a "mixed" appearance of both SLG-like and BLG-like QH plateaus in R_{12xy} [e.g., in Fig. 3(d)] observed in some of our devices (particularly at lower B, where LLs are less resolved).

In addition, hybrid QH devices have been previously realized in gate-defined p-n junctions[24,27–31] in pure SLG or BLG, where local top gates are used to create regions with different carrier densities and/or types, thus different QH states[24,27–31] (with different filling factors) in a magnetic field. The QHE observed in such p-n junctions has been successfully explained by a Landauer-Büttiker analysis of the edge states and their transmission or equilibration at the gate-defined interface between two regions with different QH states.[24,29] Asymmetric (with B or carrier types) longitudinal and Hall resistances in the QH regime have also been observed in a SLG p-n junction using a four-terminal configuration[24] instead of two-terminal configurations,[27–29] consistent with the Onsager relation. However, in a gated p-n junction, the gate-defined interface (e.g., its position, as well as its sharpness), and thus where and how the edge states from different regions meet and equilibrate, generally varies with the gate voltage. This can result in deviations of the QH plateaus from ideal quantized values (and from expected dependence on gate-tuned carrier densities), as often observed in experiments.[24,27,28,30] In our SLG-BLG junctions, the two regions with different QH states are created "naturally" because their LL structures are different (even when the two regions have the same carrier density and filling factor), allowing us to realize a QH junction with an "intrinsic" interface (defined by the edge of the second layer graphene lattice in the BLG region) and without the need of local gates (in contrast to p-n junctions in SLG or BLG[24,27–32]). The "natural" interface between SLG and BLG is fixed at the edge of the BLG lattice and more sharply defined (down to the atomic scale), making the SLG-BLG structure a potentially cleaner playground to study interface QHE in hybrid junctions. Furthermore, interface and junction QHE (dependent on the transmission and equilibration properties of edge states) can be a powerful tool to study QH edge physics.[27–29] Further improving our sample quality (e.g., using boron nitride as the substrate) may allow us to probe many interesting questions regarding the QH edge physics in the regimes of broken-symmetry QHE[33–35] or fractional QHE.[36,37] Additional and more complex device structures, such as those with extra local gates, multisegment planar junctions (e.g., SLG-BLG-SLG), or junctions involving multilayer graphene (e.g., trilayer graphene[38,39]), may also be envisioned, offering rich opportunities to study interface QHE and QH edge physics in hybrid structures involving many electronic and LL configurations.

In conclusion, we have studied the QHE of the graphene planar hybrid structures consisting of partially SLG and BLG. The interface Hall resistance exhibits quantized plateaus where the normal electron-hole and magnetic field symmetries are no longer held. Furthermore, the interface quantized Hall resistances switch between those characteristic of SLG QH states and those characteristic of BLG QH states when either the type of charge carriers or the direction of the magnetic field is revered. A Landauer-Büttiker analysis is used to explain the observed SLG-BLG interface QH states, which only depend on the chirality of the edge states. Our article offers a new system to study the physics of junction QHE in graphene hybrid structures.

We acknowledge partial financial support from the National Science Foundation (NSF), Defense Threat Reduction Agency, Miller Family Endowment, and Midwest Institute for Nanoelectronics Discovery. Part of the work was carried out at the National High Magnetic Field Laboratory, which is supported by the NSF and the State of Florida. We thank G. Jones, T. Murphy, J.-H. Park, and E. Palm for experimental assistance. Y.J. acknowledges support from NSF of China (Grant No. 11004174).

*Email address: tian5@purdue.edu
†Email address: yongchen@purdue.edu

[1] K. S. Novoselov, A. K. Geim, S. V. Morozov, D. Jiang, Y. Zhang, S. V. Dubonos, I. V. Grigorieva, and A. A. Firsov, Science **306**, 666 (2004).

[2] Y. B. Zhang, Y. W. Tan, H. L. Stormer, and P. Kim, Nature **438**, 201 (2005).

[3] K. S. Novoselov, A. K. Geim, S. V. Morozov, D. Jiang, M. I. Katsnelson, I. V. Grigorieva, S. V. Dubonos, and A. A. Firsov, Nature **438**, 197 (2005).

[4]A. K. Geim, Science **324**, 1530 (2009).
[5]A. H. Castro Neto, F. Guinea, N. M. R. Peres, K. S. Novoselov, and A. K. Geim, Rev. Mod. Phys. **81**, 109 (2009).
[6]A. S. Mayorov, R. V. Gorbachev, S. V. Morozov, L. Britnell, R. Jalil, L. A. Ponomarenko, P. Blake, K. S. Novoselov, K. Watanabe, T. Taniguchi, and A. K. Geim, Nano Lett. **11**, 2396 (2011).
[7]X. Du, I. Skachko, F. Duerr, A. Luican, and E. Y. Andrei, Nature **462**, 192 (2009).
[8]K. I. Bolotin, F. Ghahari, M. D. Shulman, H. L. Strormer, and P. Kim, Nature **462**, 196 (2009).
[9]C. R. Dean, A. F. Young, I. Meric, C. Lee, L. Wang, S. Sorgenfrei, K. Watanabe, T. Taniguchi, P. Kim, K. L. Shepard, and J. Hone, Nat. Nanotechnol. **5**, 722 (2010).
[10]K. S. Novoselov, E. McCann, S. V. Morozov, V. I. Fal'ko, M. I. Katsnelson, U. Zeitler, D. Jiang, F. Schedin, and A. K. Geim, Nat. Phys. **2**, 177 (2006).
[11]J. Velasco, Jr., L. Jing, W. Bao, Y. Lee, P. Kratz, V. Aji, M. Bockrath, C. N. Lau, C. Varma, R. Stillwell, D. Smirnov, F. Zhang, J. Jung, and A. H. MacDonald, Nat. Nanotechnol. **7**, 156 (2012).
[12]P. Maher, C. R. Dean, A. F. Young, T. Taniguchi, K. Watanabe, K. L. Shepard, J. Hone, and P. Kim, Nat. Phys. **9**, 154 (2013).
[13]R. E. Prange and S. M. Girvin, eds., *The Quantum Hall Effect*, 2nd ed. (Springer-Verlag, New York, 1990).
[14]C. P. Puls, N. E. Staley, and Y. Liu, Phys. Rev. B **79**, 235415 (2009).
[15]M. Koshino, T. Nakanishi, and T. Ando, Phys. Rev. B **82**, 205436 (2010).
[16]X. Xu, N. M. Gabor, J. S. Alden, A. M. van der Zande, and P. L. McEuen, Nano Lett. **10**, 562 (2010).
[17]A. Tsukuda, H. Okunaga, D. Nakahara, K. Uchida, T. Konoike, and T. Osada, J. Phys. Conf. Ser. **334**, 012038 (2011).
[18]Y. Zhao, Ph.D. Thesis, Columbia University, New York, NY, USA, 2012.
[19]J. F. Tian, L. A. Jauregui, G. Lopez, H. Cao, and Y. P. Chen, Appl. Phys. Lett. **96**, 263110 (2010).
[20]P. Blake, E. W. Hill, A. H. Castro Neto, K. S. Novoselov, D. Jiang, R. Yang, T. J. Booth, and A. K. Geim, Appl. Phys. Lett. **91**, 063124 (2007).
[21]A. C. Ferrari, J. C. Meyer, V. Scardaci, C. Casiraghi, M. Lazzeri, F. Mauri, S. Piscanec, D. Jiang, K. S. Novoselov, S. Roth, and A. K. Geim, Phys. Rev. Lett. **97**, 187401 (2006).
[22]S. Datta, *Electronic Transport in Mesoscopic Systems* (Cambridge University Press, Cambridge, UK, 1995).
[23]T. Ihn, *Semiconductor Nanostructures* (Oxford University Press, New York, NY, USA, 2009).
[24]D.-K. Ki, S.-G. Nam, H.-J. Lee, and B. Özyilmaz, Phys. Rev. B **81**, 033301 (2010).
[25]In Figs. 3(a) and 3(b) and Eqs. (2) and (3), we assume that $|m_1| < |m_2|$ ($m_1 \cdot m_2 > 0$). Our theoretical analysis can also be adapted to $|m_1| > |m_2|$ ($m_1 \cdot m_2 > 0$) by rotating the device in Figs. 4(a) and 4(b) by 180°. The calculated Hall resistances are then $R_{SD,ab} = h/(\max(m_1,m_2)e^2)$ and $R_{SD,ce} = h/(\min(m_1,m_2)e^2)$, and the longitudinal resistances are $R_{SD,ca} = \begin{cases} 0, \text{ CW} \\ (1/m_2 - 1/m_1)h/e^2, \text{ ACW} \end{cases}$ and $R_{SD,be} = \begin{cases} (1/m_1 - 1/m_2)h/e^2, \text{ CW} \\ 0, \text{ ACW} \end{cases}$.
[26]We point out that for Fig. 2(c), the $-h/2e^2$ plateau observed in R_{12xy} (near $V_g = 22$ V, where the SLG part has a QHE with $m_1 = -2$ and CW edge chirality but the BLG part is near its CNP and not in a QH state) is not rigorously described by our simple model in Figs. 4(a) and 4(b). However, this plateau may still be explained by a Landauer-Büttiker model by considering the entire BLG near its CNP (showing a dissipative transport with finite R_{2xx}) to act as part of the source (S) contact for SLG, resulting in $R_{12xy} = R_{1xy} = -h/2e^2$.
[27]J. R. Williams, L. Dicarlo, and C. M. Marcus, Science **317**, 638 (2007).
[28]B. Özyilmaz, P. Jarillo-Herrero, D. Efetov, D. A. Abanin, L. S. Levitov, and P. Kim, Phys. Rev. Lett. **99**, 166804 (2007).
[29]D. A. Abanin and L. S. Levitov, Science **317**, 641 (2007).
[30]D. K. Ki and H. J. Lee, Phys. Rev. B **79**, 195327 (2009).
[31]L. Jing, J. Velasco, Jr., P. Kratz, G. Liu, W. Bao, M. Bockrath, and C. N. Lau, Nano Lett. **10**, 4000 (2010).
[32]G. Liu, J. Velasco, Jr., W. Bao, and C. N. Lau, Appl. Phys. Lett. **92**, 203103 (2008).
[33]Y. Zhang, Z. Jiang, J. P. Small, M. S. Purewal, Y.-W. Tan, M. Fazlollahi, J. D. Chudow, J. A. Jaszczak, H. L. Stormer, and P. Kim, Phys. Rev. Lett. **96**, 136806 (2006).
[34]Y. Zhao, P. Cadden-Zimansky, Z. Jiang, and P. Kim, Phys. Rev. Lett. **104**, 066801 (2010).
[35]D. A. Abanin, P. A. Lee, and L. S. Levitov, Phys. Rev. Lett. **96**, 176803 (2006).
[36]C. R. Dean, A. F. Young, P. Cadden-Zimansky, L. Wang, H. Ren, K. Watanabe, T. Taniguchi, P. Kim, J. Hone, and K. L. Shepard, Nat. Phys. **7**, 693 (2011).
[37]Z.-X. Hu, R. N. Bhatt, X. Wan, and K. Yang, Phys. Rev. Lett. **107**, 236806 (2011).
[38]L. Zhang, Y. Zhang, J. Camacho, M. Khodas, and I. Zaliznyak, Nat. Phys. **7**, 953 (2011).
[39]T. Taychatanapat, K. Watanabe, T. Taniguchi, and P. Harillo-Herrero, Nat. Phys. **7**, 621 (2011).